ChemPubSoc Europe

DOI: 10.1002/slct.201800253

Chemistry SELECT Full Papers

Materials Science inc. Nanomaterials & Polymers

Molecular Insights into Benzimidazole-Linked Polymer Interactions with Carbon Dioxide and Nitrogen

Santiago Aparicio,*[a] Cafer T. Yavuz,[b] and Mert Atilhan*[c, d]

Investigation of the binding affinity gases on porous adsorbents are important for establishing understanding of effective carbon dioxide adsorption and design target specific sorbents for capturing hazardous gases for environmental protection and fuel upgrading.

A density functional theory (DFT) study that highlights the impact of benzimidazole-linked polymer structure design has been conducted to explain the molecular and electronic structure, investigate the interaction sites and elucidate the experimental results on carbon dioxide and nitrogen sorption on these porous structures. DFT calculations were used to infer the strength of the polymer – gas interaction modes as well as to quantify short-range interactions between the polymer – gas via topological characteristics analysis of intermolecular forces. Obtained results shed light on the carbon dioxide and nitrogen affinity as well as the selectivity during the adsorption process, and yet conclusions were attained on the characteristics of the adsorption type and mechanism in this study.

1. Introduction

Due to the unprecedented uses of the fossil fuels, the amount atmospheric carbon dioxide (CO_2) concentration levels have been rising and reached dangerously so-called no-turning-back limits.[1] This problem has triggered several severe effects as climate change.[2] In order to manage this environmental problem, top priority need to be given to the toxic gas emissions that are produced and released from both industrial and residential sources.[3] Clean energy sources must be considered in order to prevent the further increase of the CO_2 levels (and other toxic greenhouse gases) in the atmosphere, however until replacement of the fossil based fuels will become practical and economical, effective CO_2 capture technologies in chemical industries must be considered as an alternative to current problematic CO_2 capture methods.[4] Developing novel methods and strategies that would contribute to a decrease and control the level of toxic emissions is a crucial need and is certainly a pivotal challenge that chemical industries are facing during the last couple of decades, and thus is considered as one of the grand challenges of this century.[5] Development of an economic and sustainable alternative CO_2 capture technologies is directly related to the materials (adsorbent or absorbents) and these alternatives must be able to meet industrial requirements at actual process conditions at large scales. Such sorbents must show the characteristics of null (or minimum) toxicity,[6] low corrosivity,[7] low regeneration cost[8] and low degradation properties.[9] There is a growing interest and technical requirements in order to meet such qualifications for high-performance adsorbents, which can work based on either chemical or physical sorption mechanism. For either case, one of the most challenging issue in industrial scale for a sorbent that can be considered as an alternative in a fossil-fueled power plant (or other chemical industry that has high CO_2 emissions) is that the low CO_2 partial pressures, which requires high efficiency sorption performance in order to reduce the high capture energy penalty.[10] Which means that sorption and separation process should be based on strong either physisorption with pressure swing regeneration or chemisorption with thermal regeneration. Hence, there have been many different alternative materials have been studied such as ionic liquids,[11] deep eutectic solvents,[12] membranes,[13] metal organic frameworks,[14] covalent organic frameworks,[15] porous polymers or other porous materials.[16] Among those, covalent porous adsorbents[17] have received remarkable attention both from industry and academia over the past couple of decades since they can be custom designed and engineered to have high CO_2 sorption performance and gas separation selectivity with regeneration properties that can be achieved with low energy input in comparison to corrosive and toxic amine solutions[9c,18] Covalent porous organic polymers have structures that include attractive interaction sites that has high affinity for CO_2 with low-to-moderate binding energies that allows modest regeneration energy costs. In contrast with metal organic frameworks, amorphous covalent porous organic polymers mostly work with well-known physisorption mechanism.[19]

Having said that, in recent years there have been several studies that investigate the performance of porous polymer

[a] Prof. S. Aparicio
Department of Chemistry, University of Burgos, 09001 Burgos, Spain
E-mail: sapar@ubu.es
[b] Prof. C. T. Yavuz
Korean Advanced Institute of Science and Technology (KAIST), Daejeon, S. Korea
[c] Prof. M. Atilhan
Department of Chemical Engineering, Texas A&M University at Qatar, Doha, Qatar
E-mail: mert.atilhan@tamu.edu
[d] Prof. M. Atilhan
Gas and Fuels Research Center, Texas A&M University, College Station, TX, USA

Supporting information for this article is available on the WWW under https://doi.org/10.1002/slct.201800253

structures for gas sorption studies and these efforts are mostly concentrated on the design, synthesis and experimental aspects.[20] However, there are only a few theoretical works published in a synergistic manner that seeks the understanding of the sorption mechanism in nanoscopic approach with the comparison of an experimental data to highlight the impact of designed porous materials at the molecular and electronic levels on the CO_2 attraction and binding affinity at the molecular interaction sites. In this work, two benzimidazole-linked polymer monomers (MBI) were studied in detail for their gas sorption performances at various sorption sites via density functional theory (DFT) approach. Obtained interaction energies and topology of the electron density obtained via atom in a molecule approach were compared to experimental findings that were recently published for the same materials in order to highlight the gas sorption stabilization by MBI structure through Lewis acid–base (N···CO2) and aryl C–H···O=C=O interactions.[21] Details of the methods and the findings are given below.

2. Methods

Structures. Two MBI structures, namely MBI1 and MBI2 were considered based on previous work[21] (Figure 1) and the details

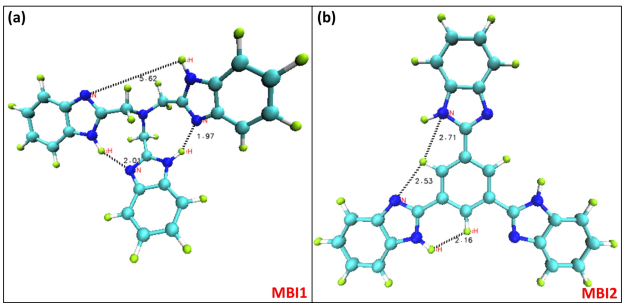

Figure 1. Final geometry of structures optimized with BLYP 6–311++G** theory level. (a) MBI1 and (b) MBI2

of the synthesis of the MBI structures are given in the ESI. Molecular clusters containing MBI1+CO_2, MBI1+N_2 MBI1+2CO_2, MBI2+CO_2, MBI2+N_2, MBI2+2CO_2 were studied by considering different CO_2 and N_2 spatial positions based on the to infer interaction properties at all logical active sites of the MBI molecules (e.g. p1, p2, p3 positions for CO_2 and N_2). For MBI-1 p1 site is N located at the center of the core structure nitrilotriacetic acid, p2 site is N(H) and p3 site is between N(H) and N located at 3,3'-diaminobenzidine. Whereas, for MBI-2, p1 site is N and p2 site is NH located at 3,3'-diaminobenzidine and p3 site is C(H) at core structure trimesic acid. Figure S1 in Supporting Information shows these selected sites.

DFT Methods. Initial structures were built by Avogadro software.[22] DFT calculations were carried out with the ORCA program.[23] All the calculations were done with the BLYP functional[24] together with the DFT–D3 method by Grimme,[25] for considering dispersion interactions, and the 6–311++G** basis set (i.e. BLYP/6- 311++G** theoretical level). The interaction energy, ΔE, for each cluster was calculated as the as the difference between the energy for the total cluster and the sum of the energies of the corresponding monomers, with the Basis Set Superposition Error (BSSE) corrected using the counterpoise procedure explained elsewhere.[26] The interaction energy values were reported in next section. Counterpoise corrected interaction energy is calculated in Equation 1 as:

$$\Delta E_{int}^{cp} = E_{sup} - \sum_{i=1}^{n} E_{m_{opt}}^{i} + \sum_{i=1}^{n}\left(E_{m_f}^{i} - E_{m_f}^{i*}\right) \quad \text{(Eq.1)}$$

where;

ΔE_{int}^{cp} is counterpoise corrected superstructure.
E_{sup} is optimized superstructure.
$E_{m_{opt}}^{i}$ is optimized single structure.
$E_{m_f}^{i}$ is optimized single structure while the coordinates are fixed at original superstructure.
$E_{m_f}^{i*}$ is optimized single structure while the coordinates are fixed at original superstructure and the other structure(s) is considered at ghost orbital state.

On the other hand, binding Energies of CO_2 and N_2 on the MBI structures were also calculated by using following Equation 2:

$$E_{bind} = E_{sup} - \sum_{i=1}^{n} E_{m_{opt}}^{i} \quad \text{(Eq.2)}$$

where;

E_{bind} is binding energy of gas molecule (CO_2 or N_2) on MBI structure.

The quantum theory of atoms in molecules (AIM) has been widely used to analyze the real space functions and characterize the type of different interactions. The topology of MBI1/2-CO_2/N_2 interactions were analyzed according to the Bader's AIM theory,[27] using the Multiwfn code.[28] Intermolecular interactions are characterized by the formation of several bond critical points (BCPs), accompanied by ring critical points (RCPs) at the center of the interaction region. Likewise, BCPs between MBI molecules and CO_2/N_2 are characterized by the values of electron density, ρ, and Laplacian of electron density, $\nabla^2\rho$. Analyzed topological values for AIM and BCP are given in Table 2.

Critical points (CP) of the charge density with inertia (3, −1) that are located between two atoms as well as the critical points (3, +1) that are often found when starting with the mean value of three charge density maxima are calculated by AIM analysis of the studied simulation results in which first the first derivative of the electron density reduces to zero from the calculated electron density ρ(r). Moreover, in order to find the type of CP that are formed in the structure, the eigenvalues are calculated. At CP, the eigenvalues of the Hessian are all real and they are mostly non-zero. The rank or the type of the CP is defined as the number of non-zero eigenvalues, depending on the values of the three eigenvalues (λ_1, λ_2, and λ_3) and the

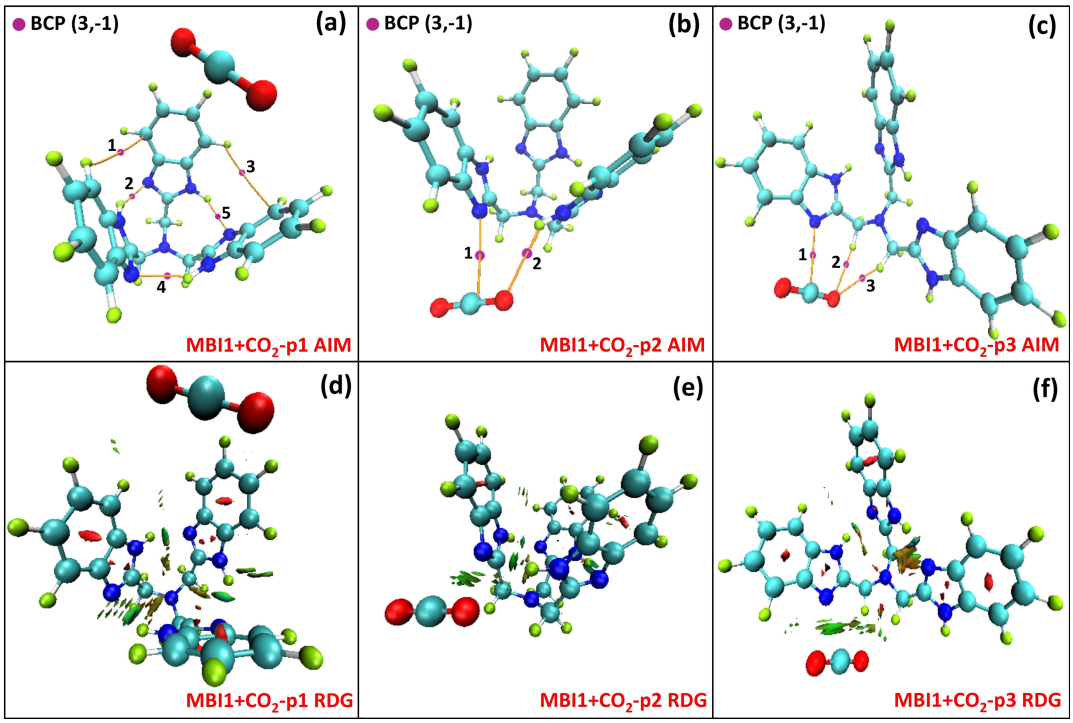

Figure 2. (a),(b),(c) Atom in Molecule (AIM) analysis of MBI1 interaction with CO_2 for P1-P2-P3 positions (explained in Figure S1, Supporting Information). Bond critical points (BCP) involving MBI1 – CO_2 interactions according to AIM are reported. Electron density (ρ) and Laplacian of electron density ($\nabla^2\rho$) for MBI1 – CO_2 BCPs are reported separately in Table 2. (d), (e), (f) Reduced Density Gradient (RDG) iso-surfaces (green or green-brown color indicates van der Waals interactions).

eigenvectors. The structures were found to be having BCP designated as (3, −1). The strength of the chemical bonds can be further studied from the location of the BCP and the electron density that is associated with the superstructure system.[29] On the other hand, one more powerful calculation tool that reconciliates the traditional Lewis model approach for the chemical bonding with the outcome of first-principles outcomes of the DFT calculations.[27,30] Based on the topological and visual analysis of the scalar fields of calculated electron density (and laplacian of the electron density), quantitative and rigorous formalisms have been quite effective in this particular issue. The reduced density gradient (RDG), is calculated in Equation 3 as:

$$s(r) = \frac{1}{2(3\pi^2)^{1/3}} \frac{|\nabla\rho(r)|}{\rho(r)^{4/3}} \qquad \text{(Eq.3)}$$

where;

$\rho(r)$ is electron density

$\nabla\rho(r)$ is laplacian of electron density

This fundamental quantity is obtained in a DFT study.

RDG has been used for developing gradient-corrected functional of increasing quality.[31] Regardless of the ρ(r) the minima of s(r) in Eq.3 have a value of 0, and it occurs whenever the ρ(r) gradient decays exponentially to zero and the $\rho(r)^{4/3}$ term approaches zero faster than $|\rho(r)|$, which happens at CPs in ρ(r). The exchange-energy weighted RDG variation with chemical association was studied by Zupan et al.[31c] previously and it was shown that RDG could be used as markers of chemical interactions by using lower energy weighted RDG values. In a different study, RDG values were associated with isosurfaces by Johnson et al. by using simpler s(r) distribution.[32] Isosurfaces were associated to the non-covalent interactions of the studied superstructure via $\rho(r)\cdot\mathrm{sign}(\lambda_2)$ quantity onto each RDG isosurface. By this method both nature and strength of the interactions are displayed in isosurface. This latter method of RDG is used in this study for studying the strength and the interaction types of MBI structures visually through the analysis of the calculated isosurfaces.

3. Results

Final optimized geometry of MBI1 and MBI2 compounds were achieved with BLYP 6–311++G** theory level and the final optimized structures for these compounds are provided in Figure 1a (MBI1) and in Figure 1b (MBI2).

Analysis of MBI – CO_2/N_2 Interaction Using DFT

Considering the subject focus of this study is to investigate the interactions of MBI compounds with gas molecules (e.g. CO_2, N_2), first we analyze the characteristics of bonding type and strength in either gas cases considering only one type of gas molecule coexist on the top of MBI adsorption sites. Figure 2

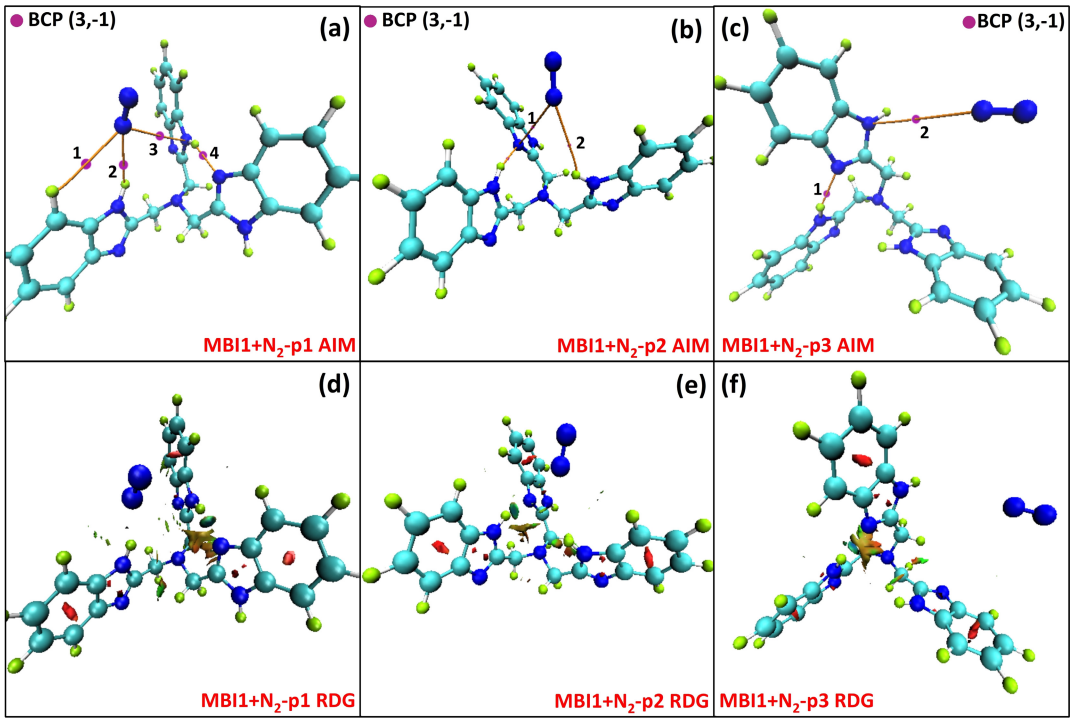

Figure 3. (a),(b),(c) Atom in Molecule (AIM) analysis of MBI1 interaction with N_2 for P1-P2-P3 positions (explained in Figure S1, Supporting Information). Bond critical points (BCP) involving MBI1 – N_2 interactions according to AIM are reported. Electron density (ρ) and Laplacian of electron density ($\nabla^2\rho$) for MBI1 – N_2 BCPs are reported separately in Table 2. (d), (e), (f) Reduced Density Gradient (RDG) iso-surfaces (green or green-brown color indicates van der Waals interactions).

shows both AIM and RDG analysis of MBI1 interaction with CO_2 and Figure 3 has the same information for MBI1 interaction with N_2 located at three different sorption sites namely p1, p2 and p3 positions (sorption sites are explained in Figure S1, Supporting Information). Figure 2 also includes the visual representations for bond critical points (BCP) for MBI1 – CO_2 interactions (type (3,–1)) according to Bader's theory,[27] which were calculated through the AIM analysis. Moreover electron density (ρ) and laplacian of electron density ($\nabla^2\rho$) for all studied DFT cases are also (Table 1).

In Figure 2 (and other figures wherever there is RDG iso-surface information) green or green-brown color indicates van der Waals type interactions between the gas molecule and the sorption site. As per the definition of hydrogen bonding according to AIM theory stands that electron density, ρ, and laplacian of electron density, $\nabla^2\rho$, must be in the range 0.002 to 0.04 a.u. and 0.020 to 0.139 a.u, respectively.[33]

There are total of 5 BCPs, 2 BCPs and 3 BCPs obtained for the MBI1-CO_2 interactions as can be seen in Figure 2a, 2b, 2c respectively. Out of these BCPs some of them show weak interaction properties when their ρ and $\nabla^2\rho$ values are considered. The strongest interaction was observed at MBI1-CO_2-p1 case at BCP#4 (BCPs are shown with purple dots in all of the figures). Nevertheless, upon close inspection of the final structure, it can be seen in Figure 2a that when CO_2 is placed on the top of the center N located at the center of the core structure of nitrilotriacetic acid, all three ligands of MBI1 is closed upwards in a umbrella-like manner and pushed CO_2 away from all of the interaction sites; and thus did not yield any BCPs for CO_2 with the any above-mentioned interaction sites of the MBI1 structure. Therefore, MBI1-CO_2-p1 is eliminated for further considerations. It would be kept in mind that the simulations that are presented herein are for the monomers that build up two MBI structures and the DFT method of choice to describe the electronic properties of the system was selected based on computationally very attractive systems applicable to mainly for short-range interactions at this level. In the case of inclusion of long-range interactions in the simulations that are prepared for a bulk polymer structure, one might expect more detailed information on the final geometry of the studied systems and how they behave in the case of interaction with gas molecules. Within the covalent porous polymers field (and also including MOFs), only a very limited number of studies are available that go beyond DFT that uses computationally very expensive post-Hartree Fock methods for bulk structure simulations that are based on configuration interaction or coupled clusters, for which the level of accuracy of a DFT simulation depends on the employment of the exchange–correlation functional. Generally speaking, in most of the cases commonly applied local functionals fail to express the long-range interactions in an accurate manner. In order to address this issue several pragmatic solutions have been suggested to remedy this deficiency in DFT approaches of such bulk simulation cases, such as the addition of a parametrised

Table 1. Electron density (ρ) and Laplacian of electron density ($\nabla^2\rho$) for MBI-1 and MBI-2.

Structure ID	BCP No.	ρ / a.u.	$\nabla^2\rho$ / a.u.	Structure ID	BCP No.	ρ / a.u.	$\nabla^2\rho$ / a.u.
MBI1-C-p1	1	0.00019	0.00280	MBI2-C-p1	1	0.00061	0.01659
	2	0.00189	0.05591		2	0.00086	0.01488
	3	0.00020	0.00292		3	0.00072	0.02102
	4	0.00189	0.05625		4	0.00214	0.04205
	5	0.00188	0.05434	MBI2-C-p2	1	0.00065	0.01769
MBI1-C-p2	1	0.00111	0.02300		2	0.00081	0.01365
	2	0.00075	0.01651		3	0.00070	0.02032
MBI1-C-p3	1	0.00122	0.02601		4	0.00216	0.04234
	2	0.00061	0.01519	MBI2-C-p3	1	0.00065	0.01785
	3	0.00071	0.01972		2	0.00079	0.01316
MBI1-N-p1	1	0.00043	0.00787		3	0.00070	0.02034
	2	0.00072	0.01427		4	0.00220	0.04295
	3	0.00020	0.00258	MBI2-N-p1	1	0.00135	0.02468
	4	0.00177	0.06520		2	0.00014	0.00163
MBI1-N-p2	1	0.00182	0.06337	MBI2-N-p2	1	0.00008	0.00081
	2	0.00020	0.00247		2	0.00000	0.00001
	3	0.00037	0.00605	MBI2-N-p3	1	0.00123	0.02306
MBI1-N-p3	1	0.00176	0.06547		1	0.00136	0.02495
	2	0.00008	0.00083		2	0.00014	0.00164
MBI1-NC-p1	1	0.00046	0.00825	MBI2-NC-p1	3	0.00217	0.04236
	2	0.00020	0.00256		4	0.00028	0.00750
	3	0.00029	0.00424		5	0.00081	0.01367
	4	0.00036	0.00593		6	0.00065	0.01763
	5	0.00161	0.03365	MBI2NC-p2	1	0.00224	0.04368
	6	0.00046	0.00748		2	0.00077	0.01264
MBI1-NC-p2	1	0.00158	0.03470		3	0.00067	0.01949
	2	0.00183	0.03748		4	0.00220	0.04297
	3	0.00004	0.00037	MBI2-NC-p3	1	0.00224	0.04368
	4	0.00047	0.00824		2	0.00068	0.01950
	5	0.00145	0.07121		3	0.00078	0.01298
MBI1-NC-p3	1	0.00482	0.00878		4	0.00059	0.01582
	2	0.00133	0.03114	MBI1-2C	1	0.00100	0.02517
	3	0.00058	0.01568		2	0.00067	0.02690
	4	0.00057	0.01382		3	0.00178	0.03554
	5	0.00061	0.01216	MBI2-2C	1	0.00110	0.02597
	6	0.00043	0.00794		2	0.00059	0.01589
	7	0.00158	0.06663		3	0.00077	0.01263
	8	0.00173	0.06593		4	0.00072	0.02101
					5	0.00242	0.04729

damped dispersion term to standard functionals. Tkatchenko and Scheffler introduced a parameter-free method to derive the interatomic coefficients entering the dispersion term.[34] and Grajciar et al. proposed a method that does not simply include a parametrised functional term to add the missing dispersion term but attempts to correct the DFT error in a systematic way.[35]

Amongst the remaining BCPs, MBI1-CO_2-p3 has shown the highest ρ and $\nabla^2\rho$ values at BCP#1 with the values of 0.00122 a.u. and 0.02601 a.u. respectively. These values are outside of the hydrogen bonding limits as mentioned above and indicating a van der Waals type of interaction between CO_2 and MBI1 structure. For MBI1-CO_2-p3, CO_2 was placed in between two identified interaction sites namely N and N(H) that are located on the ligands. It is clear that CO_2 and (N) interaction is observed in between C···N at BCP#1 for MBI1-CO_2-p3, which can also be inferred from the RDG analysis in Figure 2f (Figure 2d and Figure 2e are also provided for MBI1-CO_2-p1 and p2 cases respectively). Likewise, the presence of additional BCPs both in the space around MBI1 and CO_2 for CH(2) sites of nitrilotriacetic acid, Figure 2b and Figure 2c, show additional intermolecular interactions contributing to the stabilization of the clusters weaker than that of the mentioned BCP#1 at MBI1-CO_2-p3 case. When RDG analysis of this case is investigated, that are reported in Figure 2d,e,f intermolecular regions corresponding to the van der Waals interactions are observed. RDG spots that are green or green-brown color indicate van der Waals type interactions between the gas molecule and the sorption site. There are other obtained intermolecular regions showing additional contributions to the total interaction energy. RDG analysis of MBI1-CO_2-p3 has shown green color isosurface localization between CO_2 and N of nitrilotriacetic acid, which also confirms the highest ρ and $\nabla^2\rho$ values at BCP#1 for this case.

Similar analysis that was explained above (for MBI1-CO_2) was performed for MBI1-N2 and AIM as well as RDG results were provided In Figure 3a,b,c and Figure 3,d,e,f respectively. There are total of 4 BCPs, 3 BCPs and 2 BCPs obtained for the MBI1-N_2 interactions. When these BCPs are investigated, two cases are clearly separated from the others; MBI1-N_2-p1 (BCP#4)

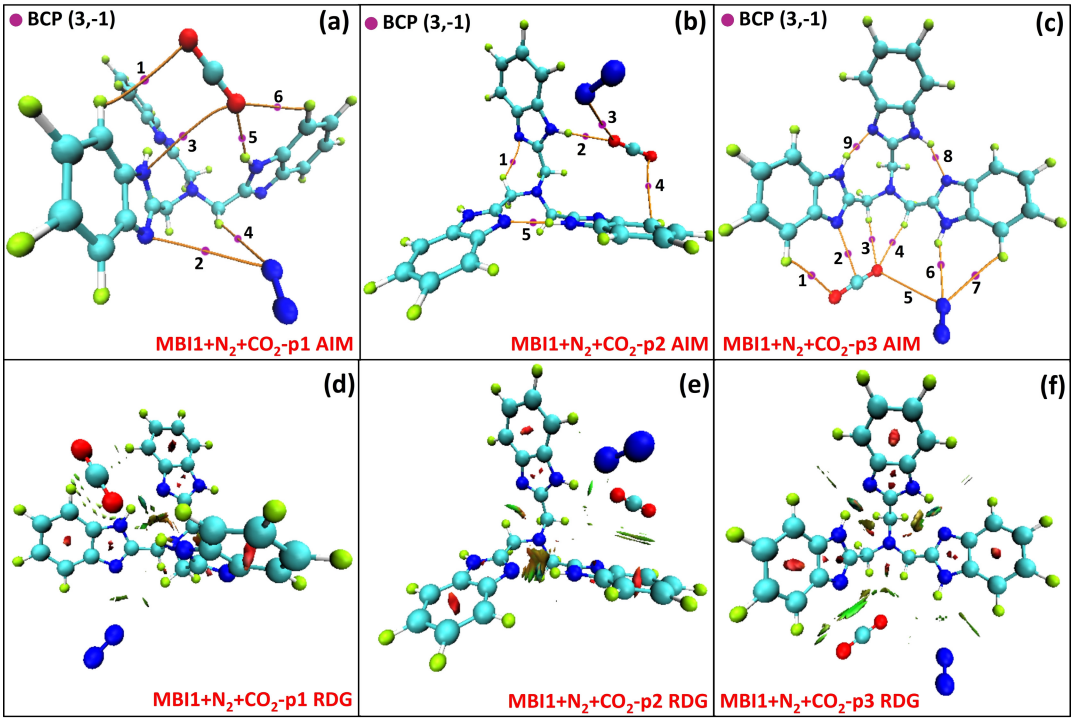

Figure 4. (a), (b), (c) Atom in Molecule (AIM) analysis of MBI1 interaction with $CO_2 + N_2$ for P1-P2-P3 positions (explained in Figure S1, Supporting Information). Bond critical points (BCP) involving MBI1 – $CO_2 + N_2$ interactions according to AIM are reported. Electron density (ρ) and Laplacian of electron density ($\nabla^2\rho$) for MBI1 – $CO_2 + N_2$ BCPs are reported separately in Table 2. (d), (e), (f) Reduced Density Gradient (RDG) iso-surfaces (green or green-brown color indicates van der Waals interactions).

and MBI1-N_2-p2 (BCP#1) with the ρ and $\nabla^2\rho$ values calculated as 0.00177 a.u., 0.06520 a.u. for MBI1-N_2-p1 (BCP#4) and 0.00182 a.u., 0.06337 a.u. for MBI1-N_2-p2 (BCP#1). However close inspection of Close inspection of the MBI1-N_2-p1 (BCP#4) show that the interaction is not in between N2 and MBI1, therefore this BCP is eliminated and leaving the strongest interaction as MBI1-N_2-p2 (BCP#1).

According to electron density values for MBI1-N_2-p2 (BCP#1), it is slightly outside the hydrogen bonding range and showing van der Waals type of binding, which is also evident from Figure 3d,e,f for all the cases of N_2 interaction with MBI1. For MBI1-N_2-p2 (BCP#1) case, the interaction is observed to be in between N≡N···N(H) at nitrilotriacetic acid. Results for AIM and RDG are given in Figures 4a,b,c and Figures 4,d,e,f respectively for the cases of both CO_2 and N_2 are placed together near to the interaction sites of MBI1. There are total of 6, 5 and 9 BCPs calculated for MBI1-NC-p1/p2/p3 cases respectively. Upon close inspection of those calculated BCPs, some of them eliminated as they do not represent the BCPs between neither CO_2 nor N_2 with MBI1 structure.

Amongst the remaining logical BCPs, in all the cases for MBI1-NC-p1/p2/p3, electron density calculated for CO_2 is much higher than that of the electron density of N_2 cases, thus showing higher interaction of MBI with CO_2 than N_2. Highest ρ was observed for CO_2 at MBI1-NC-p1 (BCP#1) case, which reveals the interaction of O=C=O···C(H)2 of the 3,3′-diaminobenzidine with 0.0046 a.u. calculated electron density. Moreover for MBI1-NC-p1 (BCP#4) case, N_2 interaction observed with C(H) at nitrilotriacetic acid with 0.00036 a.u. of electron density. This behavior is also evidenced with the RDG isosurface image given in Figure 4a, showing that localized charges between CO_2 and C(H)2 as well as CO_2 and N(H), whereas the localized charges in between N_2 and MBI is much smaller in comparison with the CO_2 case.

Similar analysis for the explaining CO_2 and N_2 with MBI2 was conducted. MBI2-CO_2 AIM results were given in Figure 5a,b,c for positions p1,p2,p3 respectively and RDG results in Figure 5d,e,f for the same positions. And for MBI2-N_2 AIM results were given in Figure 6a,b,c and RDG results in Figure 6d,e,f for the same p1,p2,p3 positions.

In the case of MBI2-CO_2 case, all of the 3 simulations that was designed CO_2 placed in three different locations initially, resulted very similar final converged structures as can be seen in Figures 5a,b,c. Snapshots of the trajectories of these simulations are provided in Figure S2 in order to show the evolution of these simulations. Close inspection of the BCPs for MBI2-CO_2 cases revealed that BCP#4 has the highest ρ and $\nabla^2\rho$ values calculated as 0.002142 a.u. and 0.04205 a.u. respectively. RDG analysis also shows van der Waals interactions between O=C=O···N(H) of the 3,3′-diaminobenzidine as linker and O=C=O···N of the and trimesic acid as core molecule. In the case of MBI2 interactions with N_2, very weak interactions were observed for MBI2-N-p2 cases. Whereas, similar interaction performance was observed for MBI2-N-p1 and MBI2-N-p3 cases,

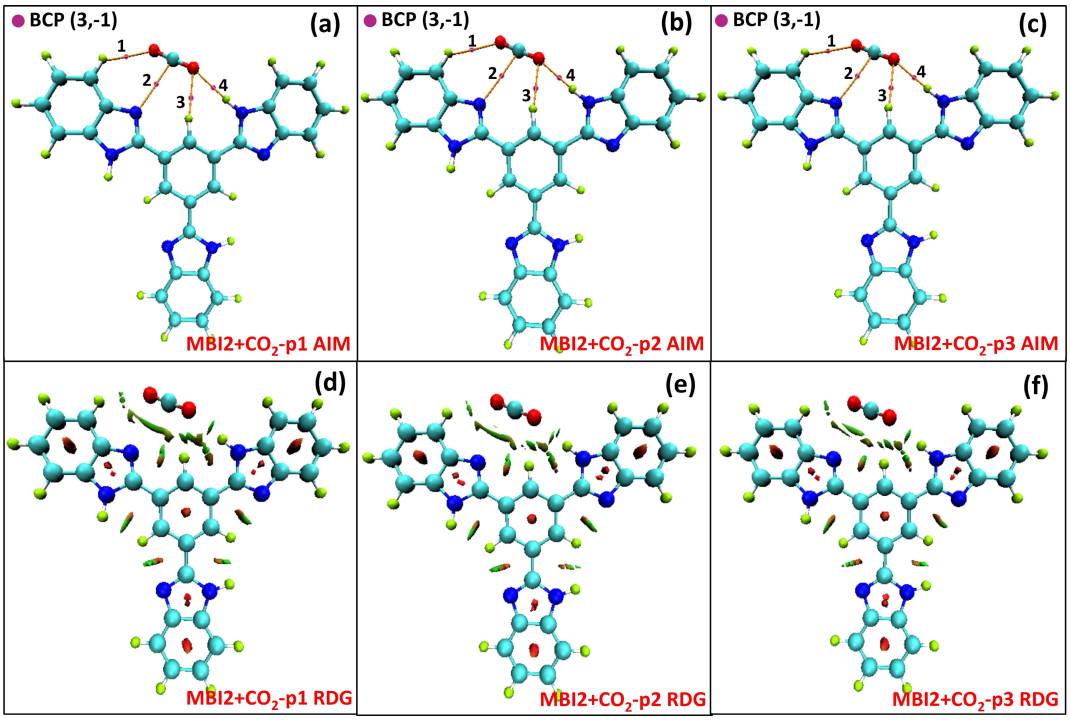

Figure 5. (a),(b),(c) Atom in Molecule (AIM) analysis of MBI2 interaction with CO_2 for P1-P2-P3 positions (explained in Figure S1, Supporting Information). Bond critical points (BCP) involving MBI2 – CO_2 interactions according to AIM are reported. Electron density (ρ) and Laplacian of electron density ($\nabla^2\rho$) for MBI2 – CO_2 BCPs are reported separately in Table 2. (d), (e), (f) Reduced Density Gradient (RDG) iso-surfaces (green or green-brown color indicates van der Waals interactions).

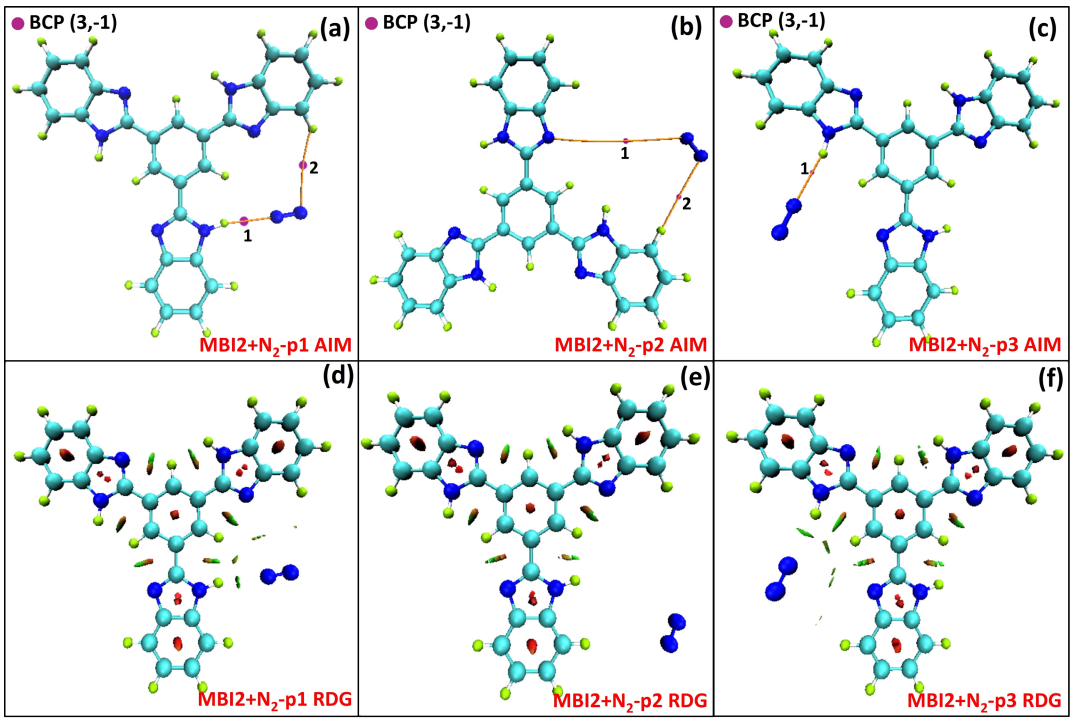

Figure 6. (a),(b),(c) Atom in Molecule (AIM) analysis of MBI2 interaction with N_2 for P1-P2-P3 positions (explained in Figure S1, Supporting Information). Bond critical points (BCP) involving MBI2 – N_2 interactions according to AIM are reported. Electron density (ρ) and Laplacian of electron density ($\nabla^2\rho$) for MBI2 – N_2 BCPs are reported separately in Table 2. (d), (e), (f) Reduced Density Gradient (RDG) iso-surfaces (green or green-brown color indicates van der Waals interactions).

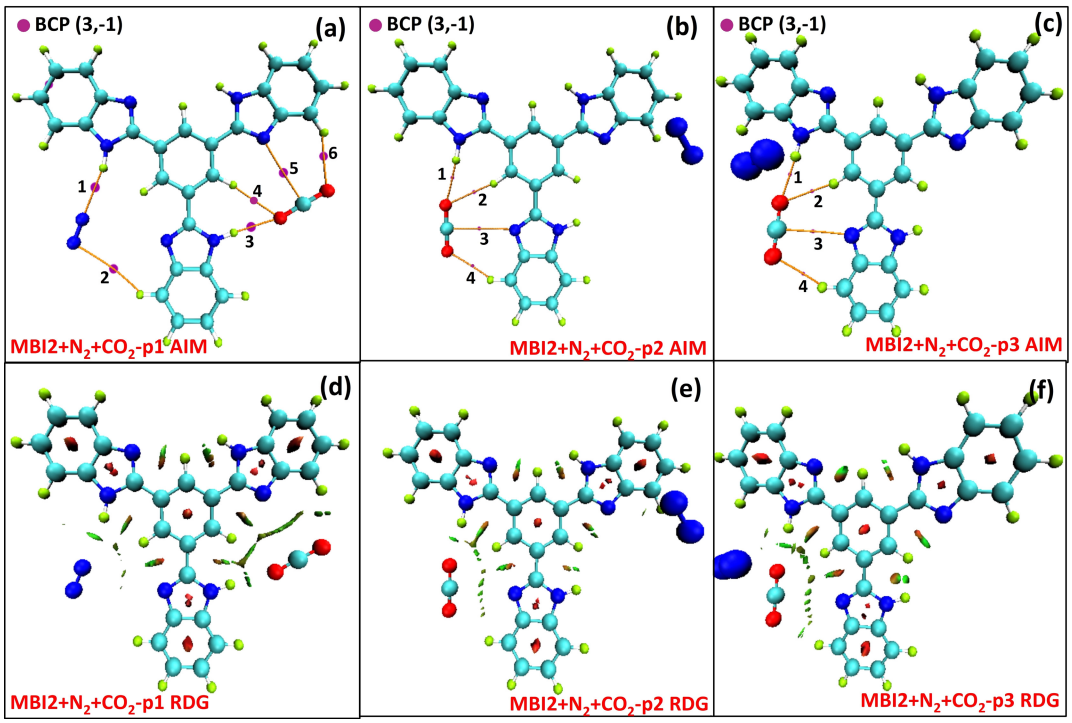

Figure 7. (a), (b), (c) Atom in Molecule (AIM) analysis of MBI2 interaction with $CO_2 + N_2$ for P1-P2-P3 positions (explained in Figure S1, Supporting Information). Bond critical points (BCP) involving MBI2 – $CO_2 + N_2$ interactions according to AIM are reported. Electron density (ρ) and Laplacian of electron density ($\nabla^2\rho$) for MBI2 – $CO_2 + N_2$ BCPs are reported separately in Table 2. (d), (e), (f) Reduced Density Gradient (RDG) iso-surfaces (green or green-brown color indicates van der Waals interactions).

especially when the N≡N···N(H) interactions are considered with the BCP values of 0.00135 a.u. for MBI2-N_2-p1 (BCP#1) and 0.00123 a.u. for MBI2-N_2-p3 (BCP#1). Other than this, N≡N···C(H)2 interactions are not noticeably high in comparison to N≡N···N(H) interactions for either cases. Other than the pure CO_2 and pure N_2 interactions with MBI2, simulations that include both CO_2 and N_2 together interacting with MBI2 were also performed to see how MBI2 would behave with gas mixture. These results were given in Figure 7a,b,c for AIM and Figure 7,d,e,f for RDG analysis. For case MBI2-NC-p2 and MBI2-NC-p3, no significant N2 interactions were observed and thus BCPs that represent N2 interactions does not exist for these 2 cases. For all the three positions, highest interactions were observed for O=C=O···N(H) with the highest ρ values calculated as 0.00217 a.u., 0.00224 a.u. and 0.00224 a.u. for MBI2-NC-p2 (BCP#3), MBI2-NC-p2 (BCP#1) and MBI2-NC-p3 (BCP#1) respectively. On the other hand, for MBI2-NC-p1 (BCP#1) shows interaction for N≡N···N(H) with the ρ values calculated as 0.00136 a.u., which is lower than the O=C=O···N(H) for the same simulation case. Therefore it can be concluded that the interaction strength for CO_2 is much higher than that of the N_2 in the same simulation conditions, when both molecules exist together near the MBI2 interaction sites. RDG analysis also coincides with the AIM findings and gives stronger interaction isosurfaces for MBI2-CO_2 than MBI2-N_2 cases (Figure 7d,e,f).

Last but not least, DFT simulations that include $2CO_2$ molecules around potential interaction sites of both MBIs were also investigated. AIM and RDG results are given for MBI1-2C and MBI2-2C cases in Figure 8a,b and Figure 8c,d respectively. CO_2 molecules were placed around MBIs in single configuration. As per the analysis of the AIM results, for both MBIs dominant interaction occurs at O=C=O···N(H), where N(H) is located on the 3,3′-diaminobenzidine ring. For MBI1-2C highest ρ value calculated at BCP#3 with the value of 0.001777 a.u. and for MBI2-2C highest ρ value calculated at BCP#5 with the value of 0.002415 a.u..

Adsorption Properties and Comparison. Results in previous section analysed using DFT methods the properties of intermolecular interactions considering the MBI clusters that contains CO_2 and N_2 around potential interaction sites. An overall picture that shows forces acting on short ranges were identified and quantified. However, in reality the effect of medium to long range interactions and the steric effects take place during the actual sorption conditions. Thus, a comparison of actual experimental data against the results that are obtained from the DFT simulations is quite important to validate the molecular level interactions. Therefore, previously reported experimental sorption data on the same MBIs were used.

The experimental data were previously published by our group and the details of the experimental procedure, uncertainties and reproducibility can be found elsewhere.[21] Experimental values are re-plotted and given in Figure S3. Binding energies for CO_2 and N_2 are also calculated by using Equation 2

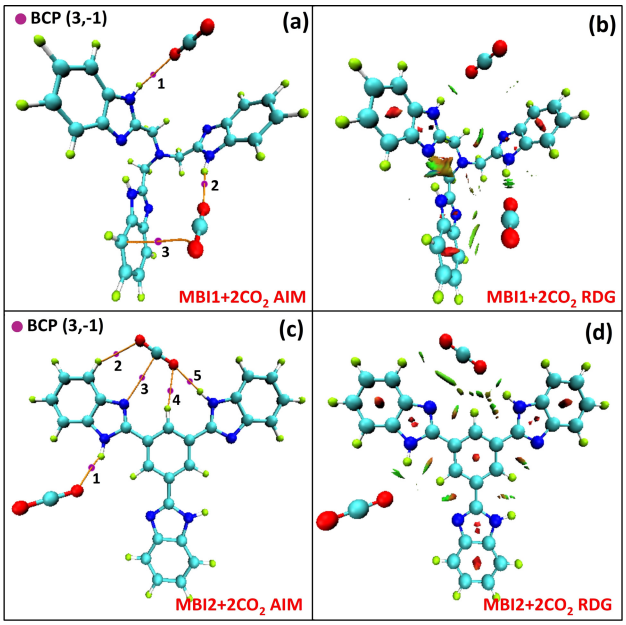

Figure 8. Panels (a), (c) Atom in Molecule (AIM) analysis of MBI1 and MBI2 interaction with $2CO_2$. Bond critical points (BCP) involving MBI2 – $2CO_2$ interactions according to AIM are reported. Electron density (ρ) and Laplacian of electron density ($\nabla^2\rho$) for MBI2 – $2CO_2$ BCPs are reported separately in Table 2. Panels (b), (d) Reduced Density Gradient (RDG) iso-surfaces (green or green-brown color indicates van der Waals interactions).

(Table 1), and these values provide the references to compare the theoretical results with the experimental data. Moreover, in Table 2 interaction energies for the studied systems are also provided.

Table 2. Counterpoise corrected interaction energies and calculated binding energies of CO_2 and N_2 on MBI-1 and MBI-2 structures.

Structure	ΔE_{int}^{cp} (eV)	E_{bind} (eV)
MBI1-C-p1	-1.975	-1.982
MBI1-C-p2	-1.993	-2.013
MBI1-C-p3	-1.831	-1.852
MBI1-N-p1	-1.061	-1.073
MBI1-N-p2	-1.051	-1.068
MBI1-N-p3	-1.066	-1.072
MBI1-NC-p1	-2.965	-3.003
MBI1-NC-p2	-2.976	-3.009
MBI1-NC-p3	-3.004	-3.036
MBI1-2C	-3.755	-3.795
MBI2-C-p1	-1.981	-2.002
MBI2-C-p2	-1.983	-2.004
MBI2-C-p3	-1.980	-2.002
MBI2-N-p1	-1.167	-1.167
MBI2-N-p2	-1.105	-1.126
MBI2-N-p3	-1.166	-1.167
MBI2-NC-p1	-3.171	-3.172
MBI2-NC-p2	-3.115	-3.136
MBI2-NC-p3	-3.127	-3.137
MBI2-2C	-3.911	-3.911

For an economic CO_2 mitigation strategies, desorption mechanism of CO_2 from an adsorbed surface must be investigated carefully. The captured CO_2 can be permanently sequestered in various different scenarios depending on desorption performance, such as catalytic conversion to other useful chemicals (fuels and reagents) as well as direct injection to either depleted reservoirs or geological formations with the aim of maintaining reservoir pressures (e.g. enhanced oil/gas recovery applications). In the case of physical adsorbents, determinations of physical limitations on desorption as important as adsorption and it is standing as one of the main hurdle for a material to be considered as viable alternative. Desorption mechanism is studied by investigating binding affinity of porous sorbents. In the case of physical adsorbents, captured CO_2 can be desorbed with a low energy cost by depressurization without applying additional heat. Whereas in the case of chemisorption desorption via heating is a known practice as it is essential to break the bonds between the adsorbate and adsorbent. Nevertheless, there is a trade-off between the low binding energy of porous polymers (or adsorbents in general) and the CO_2 sorption performance. Lower the binding energy lower the CO_2 sorption performance, which can be modified via carefully designed functionalization of the pores with the "CO_2-philic" groups in order to enhance the binding energies, as it is the main framework of this study to investigate different functionalizations for benzimidazole linked structures. It is a known fact that utilization of polar functional groups such as –OH, $–NH_2$, $–NO_2$ and $–SO_3H$ would enhance the CO_2 capture performance of a porous adsorbents through hydrogen bonding and dipole-quadrupole interactions. In order to study the binding energies experimentally, isosteric enthalpies of adsorption (Q_{st} kJ·mol^{-1}) are calculated and reported elsewhere. From this information comments on sorption performances and selectivity's for different gases can be inferred for further performance evaluation. For instance in a recent study by Altarawneh,[36] studied benzimidazole linked porous structures and their performance on binding of small gases (e.g., N_2, CO_2, and CH_4), they also linked pure gas uptake isotherms and selectivity to binding affinity (Qst) for studied gases. In this work binding energy and sorption performance is reported as lower the binding energy higher the sorption performance. Moreover, in the same study when different gases are compared, similar behavior is also observed on the binding energy vs sorption performance relation. In a different study again by Altarawneh,[17a] Q_{st} for CO_2 was calculated via virial method and compared with the estimated binding energies via DFT calculations. Authors reported on the Q_{st} as it has the highest value at zero coverage then start to drop as the sorption continues. It can be inferred from these findings that initial observed high Q_{st} are driven by favorable interactions between the active sites and the gas molecules and as these active sites become less available and accessible for the gas molecules Qst value decreases in parallel to gas loading increase. In this presented work, when binding energy values are analyzed, for both MBI cases it is observed that the binding energies for CO_2 are higher than that of the N_2. Experimental results also inline with this finding and as can be seen in

Figure S3 that for both MBI cases CO_2 sorption performance is higher than the N_2 sorption performance.

Moreover, these findings are also inline with the topological findings in previous section, where electron density values at the BCPs between the MBIs and CO_2 are mostly higher than the N_2 cases. In the case of MBI-2C cases, the binding energy for MBI2-2C is calculated as −3.91 eV whereas the MBI1-2C is calculated as −3.80 eV, which also confirms the superior sorption performance of MBI2 against MBI1 as a result of detailed experimental studies. The reported results show that both the MBIs are able to develop stronger interaction with CO_2 than N_2 with the existence of the N and N(H) interaction sites in the imidazole ring. Moreover, the it is also observed that the C(H)2 sites located in the trimesic acid of MBI2 has enhanced CO_2 binding in MBI2 more than the N site located in nitrilotriacetic acid in MBI1; and this is also confirmed with the experimental data.

4. Conclusions

The sorption properties of two benzimidazole-linked polymers were studied by using density functional theory calculations. The systems containing both CO_2 and N_2 were considered at various different sorption sites and the simulations obtained for these cases were analysed in terms of microscopic structure, intermolecular forces, weak or strong bonding locations and topological behaviours. It was observed that the CO_2 interactions are enhanced with the existence of the imidazole ring attached to these systems (in 3,3′-diaminobenzidine), which is highly polar and carries a net dipole moment. Whereas CO_2 is highly symmetric and has a permanent electric quadruple, which are pointing opposite directions. The analyzed interactions can be attributed due to the interaction between the MBIs and the CO_2 molecules through the dipole-quadruple interactions. It shall also be noted that the similar interaction patterns have been noted and authenticated by comparisons through the experimental findings for the same MBIs. The RGD isosurfaces between MBI and CO_2 (and N_2) molecules show effective van der Waals interactions for all the studied cases. Larger interaction energies and RDG isosurfaces for O=C=O···N(H) were observed at the imidazole ring in comparison with the other interactions sites.

Overall, our study reveals that MBI offer various interaction sites for both CO_2 and N_2, and along with their internal energies as well as binding energies, and thus a clear explanation on the high-pressure sorption experimental data was revealed via using density functional theory simulations and calculations. As future contributions, there are several works is in progress in order to extend this analysis to other types porous polymer structures including covalent organic polymers and frameworks that contains complexes with multiple interaction sites surrounded with multiple gas molecules, with the ultimate purpose obtaining first principle calculations on the properties of the interactions, interaction regions, quantification of interatomic potentials as well as the binding energies.

Supporting Information Summary

Supporting information includes MBI1 and MBI2 structures and active site positions that are considered for CO_2 and N_2 locations in DFT simulations, snapshots for MBI2-C-p2 and MBI2-C-p3 trajectory files and experimental sorption data for CO_2 and N_2 on MBI1 and MBI2.

Acknowledgement

This work was funded by Junta de Castilla y León (Spain, project BU324U14). We also acknowledge The Foundation of Supercomputing Center of Castile and León (FCSCL, Spain) for providing supercomputing facilities. The statements made herein are solely the responsibility of the authors.

Conflict of Interest

The authors declare no conflict of interest.

Keywords: Atom in a Molecule (AIM) · Benzimidazole-linked polymers · Density functional theory (DFT) · Gas Capture · Gas Storage

[1] a) R. Monastersky, *Nature* **2013**, *497*, 13–14; b) R. B. Jackson, J. G. Canadell, C. Le Quéré, R. M. Andrew, J. I. Korsbakken, G. P. Peters, N. Nakicenovic, *Nat. Clim. Change* **2015**, *6*, 7.

[2] a) G. P. Peters, R. M. Andrew, T. Boden, J. G. Canadell, P. Ciais, C. Le Quéré, G. Marland, M. R. Raupach, C. Wilson, *Nat. Clim. Change* **2012**, *3*, 4; b) *IPCC, 2014: Climate Change 2014: Synthesis Report. Contribution of Working Groups I, II and III to the Fifth Assessment Report of the Intergovernmental Panel on Climate Change [Core Writing Team, R. K. Pachauri and L. A. Meyer (eds.)]. IPCC, Geneva, Switzerland, 151 pp.*

[3] T. P. Senftle, E. A. Carter, *Acc. Chem. Res.* **2017**, *50*, 472–475.

[4] a) J. D. Steven, H. S. Robert, *Environ. Res. Lett.* **2014**, *9*, 084018; b) R. N. Echevarria-Huaman, T. X. Jun, *Renewable Sustainable Energy Rev.* **2014**, *31*, 368–385; c) D. S. Sholl, R. P. Lively, *Nature* **2016**, *532*, 435–437.

[5] a) S. Chu, *Science* **2009**, *325*, 1599; b) S. Chu, Y. Cui, N. Liu, *Nat. Mater.* **2016**, *16*, 16; c) B. Smit, A.-H. A. Park, G. Gadikota, *Front. Ener. Res.* **2014**, *55*.

[6] E. Gjernesa, L. I. Helgesena, Y. Mareeb, *Energy Procedia* **2013**, *37*, 735–742.

[7] a) J. Kittel, R. Idem, D. Gelowitz, P. Tontiwachwuthikul, G. Parrain, A. Bonneau, *Energy Procedia* **2009**, *1*, 791–797; b) J. Kittel, E. Fleury, B. Vuillemin, S. Gonzalez, F. Ropital, R. Oltra, *Mater. Corros.* **2012**, *63*, 223–230; c) A. Rafat, M. Atilhan, R. Kahraman, *Ind. Eng. Chem. Res.* **2016**, *55*, 446–454.

[8] a) A. B. Rao, E. S. Rubin, *Ind. Eng. Chem. Res* **2006**, *45*, 2421–2429; b) J. Husebye, A. L. Brunsvold, S. Roussanaly, X. Zhang, *Energy Procedia* **2012**, *23*, 381–390; c) A. S. E. Nasr, T. Nelson, M. R. M. Abu-Zahra, *Energy Procedia* **2013**, *37*, 2432–2442; d) M. Vaccarelli, R. Carapellucci, L. Giordano, *Energy Procedia* **2014**, *45*, 1165–1174; e) G. Manzolini, E. Sanchez Fernandez, S. Rezvani, E. Macchi, E. L. V. Goetheer, T. J. H. Vlugt, *Appl. Energy* **2015**, *138*, 546–558.

[9] a) D. Cebrucean, V. Cebrucean, I. Ionel, *Energy Procedia* **2014**, *63*, 18–26; b) D. Bhattacharyya, D. C. Miller, *Curr. Opin. Chem. Eng.* **2017**, *17*, 78–92; c) D. J. Heldebrant, P. K. Koech, V.-A. Glezakou, R. Rousseau, D. Malhotra, D. C. Cantu, *Chem. Rev.* **2017**, *117*, 9594–9624.

[10] J. A. A. Gibson, E. Mangano, E. Shiko, A. G. Greenaway, A. V. Gromov, M. M. Lozinska, D. Friedrich, E. E. B. Campbell, P. A. Wright, S. Brandani, *Ind. Eng. Chem. Res.* **2016**, *55*, 3840–3851.

[11] S. Zeng, X. Zhang, L. Bai, X. Zhang, H. Wang, J. Wang, D. Bao, M. Li, X. Liu, S. Zhang, *Chem. Rev.* **2017**, *117*, 9625–9673.

[12] a) G. García, S. Aparicio, R. Ullah, M. Atilhan, *Energy Fuels* **2015**, *29*, 2616–2644; b) S. Sarmad, J.-P. Mikkola, X. Ji, *ChemSusChem* **2017**, *10*, 324–352.
[13] S. Rafiq, L. Deng, M.-B. Hägg, *ChemBioEng Rev.* **2016**, *3*, 68–85.
[14] a) J. Yu, L.-H. Xie, J.-R. Li, Y. Ma, J. M. Seminario, P. B. Balbuena, *Chem. Rev.* **2017**, *117*, 9674–9754; b) H. Li, M. Eddaoudi, M. O'Keeffe, O. M. Yaghi, *Nature* **1999**, *402*, 276.
[15] a) H. A. Patel, F. Karadas, A. Canlier, J. Park, E. Deniz, Y. Jung, M. Atilhan, C. T. Yavuz, *J. Mater. Chem.* **2012**, *22*, 8431–8437; b) Y. Zeng, R. Zou, Y. Zhao, *Adv. Mater.* **2016**, *28*, 2855–2873.
[16] a) A. P. Côté, H. M. El-Kaderi, H. Furukawa, J. R. Hunt, O. M. Yaghi, *J. Am. Chem. Soc.* **2007**, *129*, 12914–12915; b) M. G. Rabbani, H. M. El-Kaderi, *Chem. Mater.* **2012**, *24*, 1511–1517.
[17] a) S. Altarawneh, S. Behera, P. Jena, H. M. El-Kaderi, *Chem. Commun.* **2014**, *50*, 3571–3574; b) K. Sumida, D. L. Rogow, J. A. Mason, T. M. McDonald, E. D. Bloch, Z. R. Herm, T.-H. Bae, J. R. Long, *Chem. Rev.* **2012**, *112*, 724–781; c) R. Dawson, A. I. Cooper, D. J. Adams, *Prog. Polym. Sci.* **2012**, *37*, 530–563.
[18] R. S. Haszeldine, *Science* **2009**, *325*, 1647.
[19] A. H. Berger, A. S. Bhown, *Energy Procedia* **2011**, *4*, 562–567.
[20] a) J.-X. Jiang, F. Su, A. Trewin, C. D. Wood, H. Niu, J. T. A. Jones, Y. Z. Khimyak, A. I. Cooper, *J. Am. Chem. Soc.* **2008**, *130*, 7710–7720; b) S. Bandyopadhyay, A. G. Anil, A. James, A. Patra, *ACS Appl. Mater. Interfaces* **2016**, *8*, 27669–27678; c) M. Atilhan, S. Atilhan, R. Ullah, B. Anaya, T. Cagin, C. T. Yavuz, S. Aparicio, *J. Chem. Eng. Data* **2016**, *61*, 2749–2760; d) O. Buyukcakir, Y. Seo, A. Coskun, *Chem. Mater.* **2015**, *27*, 4149–4155; e) R. Ge, D. Hao, Q. Shi, B. Dong, W. Leng, C. Wang, Y. Gao, *J. Chem. Eng. Data* **2016**, *61*, 1904–1909; f) J.-X. Hu, H. Shang, J.-G. Wang, L. Luo, Q. Xiao, Y.-J. Zhong, W.-D. Zhu, *Ind. Eng. Chem. Res.* **2014**, *53*, 11828–11837; g) H. A. Patel, D. Ko, C. T. Yavuz, *Chem. Mater.* **2014**, *26*, 6729–6733; h) M. Saleh, J. N. Tiwari, K. C. Kemp, M. Yousuf, K. S. Kim, *Environ. Sci. Technol.* **2013**, *47*, 5467–5473; i) D. Thirion, Y. Kwon, V. Rozyyev, J. Byun, C. T. Yavuz, *Chem. Mater.* **2016**, *28*, 5592–5595; j) R. Ullah, M. Atilhan, B. Anaya, S. Al-Muhtaseb, S. Aparicio, H. Patel, D. Thirion, C. T. Yavuz, *ACS App. Mater. Interfaces* **2016**, *8*, 20772–20785; k) X. Zhu, C. Tian, G. M. Veith, C. W. Abney, J. Dehaudt, S. Dai, *J. Am. Chem. Soc.* **2016**, *138*, 11497–11500.
[21] R. Ullah, M. Atilhan, A. Diab, E. Deniz, S. Aparicio, C. T. Yavuz, *Adsorption* **2016**, *22*, 247–260.
[22] S. Adams, P. de Castro, P. Echenique, J. Estrada, M. D. Hanwell, P. Murray-Rust, P. Sherwood, J. Thomas, J. A. Townsend, *J. Cheminf.* **2011**, *3*.
[23] F. Neese, *Wiley Interdisciplinary Reviews: Computational Molecular Science* **2012**, *2*, 73–78.
[24] a) C. Lee, W. Yang, R. G. Parr, *Phys. Rev. B* **1988**, *37*, 785–789; b) A. D. Becke, *Phys. Rev. A* **1988**, *38*, 3098–3100.
[25] S. Grimme, J. Antony, S. Ehrlich, H. Krieg, *J. Chem. Phys.* **2010**, *132*, 154104.
[26] S. Simon, M. Duran, J. J. Dannenberg, *J. Chem. Phys.* **1996**, *105*, 11024–11031.
[27] R. F. W. Bader, *Atoms in Molecules: a Quantum Theory*, Oxford University Press, **1990**.
[28] T. Lu, F. Chen, *J. Comput. Chem.* **2012**, *33*, 580–592.
[29] a) J. Xiao, Y.-P. Zhao, X. Fan, J.-P. Cao, G.-J. Kang, W. Zhao, X.-Y. Wei, *Fuel Process. Technol.* **2017**, *168*, 58–64; b) V. Anbu, K. A. Vijayalakshmi, R. Karunathan, A. D. Stephen, P. V. Nidhin, *Arabian J. Chem.* **2016**.
[30] B. Silvi, A. Savin, *Nature* **1994**, *371*, 683.
[31] a) G. Saleh, C. Gatti, L. Lo Presti, *Comput. Theor. Chem.* **2012**, *998*, 148–163; b) A. Zupan, J. P. Perdew, K. Burke, M. Causà, *Int. J. Quantum Chem.* **1997**, *61*, 835–845; c) A. Zupan, K. Burke, M. Ernzerhof, J. P. Perdew, *J. Chem. Phys.* **1997**, *106*, 10184–10193.
[32] E. R. Johnson, S. Keinan, P. Mori-Sánchez, J. Contreras-García, A. J. Cohen, W. Yang, *J. Am. Chem. Soc.* **2010**, *132*, 6498–6506.
[33] H. Roohi, A.-R. Nowroozi, E. Anjomshoa, *Comput. Theor. Chem.* **2011**, *965*, 211–220.
[34] a) A. Tkatchenko, R. A. DiStasio, R. Car, M. Scheffler, *Phys. Rev. Lett.* **2012**, *108*, 236402; b) A. Tkatchenko, M. Scheffler, *Phys. Rev. Lett.* **2009**, *102*, 073005.
[35] L. Grajciar, O. Bludský, P. Nachtigall, *J. Phys. Chem. Lett.* **2010**, *1*, 3354–3359.
[36] S. Altarawneh, T. İslamoğlu, A. K. Sekizkardes, H. M. El-Kaderi, *Environ. Sci. Technol.* **2015**, *49*, 4715–4723.

Submitted: January 29, 2018
Revised: March 20, 2018
Accepted: March 20, 2018